Dicle University
Journal of Engineering
https://dergipark.org.tr/tr/pub/dumf
duje.dicle.edu.tr

Research Article

Development of an Equivalent Circuit Topology for a Directional Coupler

İbrahim GENÇ[1,2], Mahmut Ahmet GÖZEL[3], Mesud KAHRİMAN[4*]

[1] Isparta University of Applied Sciences, Yalvaç Technical Sciences Vocational School -Yalvaç 32400 Isparta, Turkiye ibrahimgenc@isparta.edu.tr, Orcid No: 0000-0002-1693-6685

[2] Suleyman Demirel University, Faculty of Engineering and Natural Sciences, Electrical-Electronics Engineering Department, Isparta, Turkiye, d2240112901@ogr.sdu.edu.tr, Orcid No: 0000-0002-1693-6685

[3] Suleyman Demirel University, Faculty of Engineering and Natural Sciences, Electrical-Electronics Engineering Department, Isparta, Turkiye, mahmutgozel@sdu.edu.tr, Orcid No: 0000-0002-0360-7188

[4] Suleyman Demirel University, Faclty of Engineering and Natural Sciences, Electrical-Electronics Engineering Department, Isparta, Turkiye, mesudkahriman@sdu.edu.tr, Orcid No: 0000-0003-0731-0936

ARTICLE INFO

Article history:

Received 8 February 2026
Received in revised form 6 April 2026
Accepted 8 April 2026
Available online 18 July 2026

Keywords:

Directional Coupler, Equivalent Circuit Topology, Transmission Line Theory, Microwave Design

Doi: 10.24012/dumf.1884058

* Corresponding author

ABSTRACT

In the design and analysis processes of microstrip directional couplers, full-wave electromagnetic simulations provide high accuracy. Still, they require high computational costs, especially in broadband optimization and system-level designs. This study presents an improved lumped element equivalent circuit topology based on the segmentation principle in transmission line theory, which enables the rapid and accurate modeling of the distributed electromagnetic behavior of physical structures. Within the scope of this study, the performance of different circuit topologies designed in the ADS environment was comparatively analyzed using reference *S*-parameters obtained with CST Studio Suite. In optimization processes, it has been observed that the physical behavior of fundamental π models is determined by the reflection coefficient (S_{11}), though phase and amplitude errors increase at high frequencies. To overcome this limitation, a final topology was developed by dividing the connecting lines into multiple LC sections and modeling the structural effects. Analysis results show that the Mean Absolute Error value, which was 4.52 dB in the basic models, was reduced to 0.67 dB in the proposed final topology. In particular, the low error rate of 0.64 dB obtained in the transmission characteristic proves that the developed model successfully represents the physical structure over a wide band range. The presented approach combines the accuracy of electromagnetic analysis with the speed of circuit simulation, offering an effective solution for designing complex microwave systems.

Introduction

In modern microwave communication systems, radar technologies, and precision measurement systems, the splitting, sampling, and monitoring of signal power are critical processes that directly affect system performance. Passive microwave components that perform these functions include directional couplers, feedback control in power amplifiers, antenna feed networks, and modulator circuits, which are fundamental building blocks with a wide range of applications [1, 2]. Microstrip technology, on the other hand, is the most commonly used transmission line infrastructure in the design of these components due to its planar structure, low production cost, and high integration with active circuit elements.

However, the inhomogeneous dielectric medium inherent in the microstrip structure (air-dielectric interface) differentiates the phase velocities in the dual and single modes of the electromagnetic wave ($v_{even} \neq v_{odd}$), leading to suboptimal directivity in the designed directional couplers and a decrease in insulation performance. [3, 4]. Therefore, correctly predicting these electromagnetic (EM) effects and non-ideal behaviors during the design phase is critically important for the designer.

Today, the design and analysis of these structures are mostly being performed using full-wave electromagnetic simulation tools (CST Studio Suite, HFSS, etc.). Although these tools provide high accuracy, they create a high computational load in wideband optimizations and comprehensive parametric scans, resulting in significant time loss [5]. Furthermore, since EM simulations often treat the physical structure as a “black box,” it is usually quite difficult for the designer to determine which specific EM interaction is responsible for the performance losses observed in the *S*-parameter results.

Therefore, the creation of an electrical equivalent circuit model for a physical microwave structure is based on three fundamental reasons, as emphasized in the literature: Physical Insight; equivalent circuit models provide deep physical insight into the behavior of the structure by converting electromagnetic field interactions (electrical and magnetic couplings) into more easily understandable collective circuit elements. This can directly identify the source of performance-limiting effects [6]. *Computational Efficiency*; while the EM analysis of a complex structure can take hours, the simulation of an appropriately modeled lumped element equivalent circuit can be completed in seconds [6]. *System Integration*; SPICE (Simulation Program for Integrated Circuits)-compatible equivalent circuit models offer much faster convergence and easier integration compared to *S*-parameter blocks, enabling the use of directional couplers in time-domain analysis alongside active circuits such as power amplifiers [7]. In recent literature, such lumped-element equivalent circuit modeling, miniaturization, and multi-section techniques have also been highly effective in the theoretical analysis and development of other compact passive microwave components, such as Wilkinson power dividers [8], [9].

In this study, a broadband and high-accuracy electrical equivalent circuit topology has been developed for a physically designed microstrip directional coupler. Within the scope of the study, based on reference data obtained from the electromagnetic simulation of the physical structure using Computer Simulation Technology (CST) Studio Suite, the new equivalent circuit topology representing the electromagnetic behavior of the structure with lumped elements has been optimized in the Advanced Design System (ADS) environment.

Basic Equivalent Circuit Topology for Directional Couplers

A transmission line segment can be modeled using equivalent circuits of the "T" or "π" type, constructed with lumped elements [10]. The validity of this lumped element approach relies on the physical length (l) of the represented line being electrically short ($l<<\lambda_g$) relative to the wavelength (λ_g) at the operating frequency [10]. Figure 1 shows the basic "π" type equivalent circuit model of a transmission line at frequency f_0 with characteristic impedance Z_0 and electrical length θ.

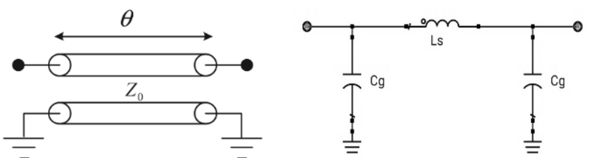

(a) (b)

Figure 1. (a) Transmission line segment with characteristic impedance Z_0 and electrical length θ (b) "π" type equivalent circuit model [7].

Figure 1. (b) shows the inductance effect of the transmission line L_s, while C_g represents the capacitance formed between the transmission line and the ground plane. These element values can be computed using the following equations [7].

$$L_s = \frac{Z_0}{2\pi f_0} Sin\theta \tag{1}$$

$$C_g = \frac{1 - cos\theta}{2\pi f_0 Z_0 sin\theta} \tag{2}$$

The basic structure of a microstrip directional coupler, as shown in Figure 2, consists of two transmission lines placed at a close distance to each other. This physical proximity between the lines induces mutual interaction of electromagnetic fields between the two lines. This interaction can be attributed to two fundamental physical mechanisms: first, the capacitive coupling (C_c) effect, which arises from the potential difference between the lines and is caused by electric field leakage; second, the mutual inductance (M) effect, which occurs when the magnetic flux generated by the current in one line cuts through the other line.

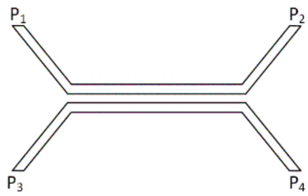

Figure 2. Basic geometric structure of the directional coupler.

In the literature, the standard method used for analyzing directional couplers is the "dual and single mode" analysis detailed in the fundamental sources. This approach divides complex EM fields into two simple symmetric cases. The dual mode, where both lines are excited in phase, and the single mode, where the lines are excited in opposite phases. These two modes have different characteristic impedances, known as the even mode impedance (Z_{0e}) and the odd mode impedance (Z_{0o}), respectively. The fundamental performance parameters of a directional coupler, the coupling factor (C) and characteristic impedance (Z_0), are directly determined by the relationship and difference between these two mode impedances [8, 9]. The Z_{0e} and Z_{0o} impedances of a unidirectional coupler with a known coupling factor and characteristic impedance can be calculated using Equation (3) and Equation (4) [12].

$$Z_{0e} = Z_0 \sqrt{\frac{1 + 10^{C/20}}{1 - 10^{C/20}}} \tag{3}$$

$$Z_{0o} = Z_0 \sqrt{\frac{1 - 10^{C/20}}{1 + 10^{C/20}}} \tag{4}$$

To create a complete equivalent circuit model of the directional coupler based on physical reality, it is necessary to model the transmission characteristics of each line and also integrate the capacitive and inductive coupling interactions between these two lines into the model. The basic equivalent circuit topology that meets these requirements and that is well accepted in the literature is shown in Figure 3 [7].

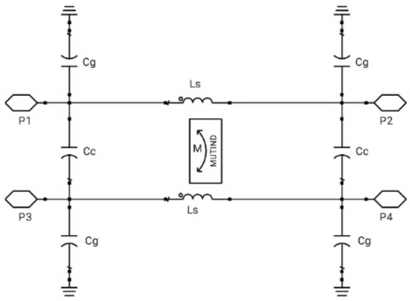

Figure 3. Basic equivalent circuit of the directional coupler.

In the equivalent circuit shown in Figure 3, L_s represents the inductance of the coupling lines, M shows the mutual interaction of these inductances, C_c denotes the coupling capacitance between the coupling lines, and C_g indicates the capacitance formed between the coupling lines and the ground plane. The values of these collective elements can be determined directly using the following equations, which utilize the characteristic parameters Z_{0e} and Z_{0o} of the line [7].

$$C_g = \frac{1}{2\pi f_0 Z_{0e}} \quad (5)$$

$$C_c = \frac{1}{4\pi f_0}\left(\frac{1}{Z_{0o}} - \frac{1}{Z_{0e}}\right) \quad (6)$$

$$L_s = \frac{Z_{0e} + Z_{0o}}{4\pi f_0} \quad (7)$$

$$M = \frac{Z_{0e} - Z_{0o}}{4\pi f_0} \quad (8)$$

Development of a Directional Coupler Equivalent Circuit Topology

Modeling the electromagnetic behavior of microstrip directional couplers across a wide frequency band using lumped element equivalent circuits is one of the most critical stages of the design process. Full-wave electromagnetic simulation tools comprehensively calculate all complex physical interactions within the structure, mode dispersions, scattering fields, and distributed coupling mechanisms based on Maxwell's equations. However, simple circuit topologies consisting of basic inductance and capacitance elements are insufficient to represent these distributed electromagnetic effects, especially at high frequencies [13]. Therefore, to achieve a high degree of agreement between the simulation data of the physical structure and the circuit model, it is necessary to go beyond standard models and devise an advanced circuit topology that also encompasses structural electromagnetic effects.

The geometric structure and dimensions of the directional coupler, for which the equivalent circuit topology is to be developed, are shown in Figure 4. The frequency dependence of the S parameters obtained from electromagnetic simulations performed in the CST environment is shown in Figure 5 [14]. The objective of this study is to convert the reflection (S_{11}), transmission (S_{21}), coupling (S_{31}), and isolation (S_{41}) behaviors obtained from CST-based full-wave simulations into an equivalent circuit model that offers high physical realism and fast simulation capabilities, created using lumped elements in the ADS environment.

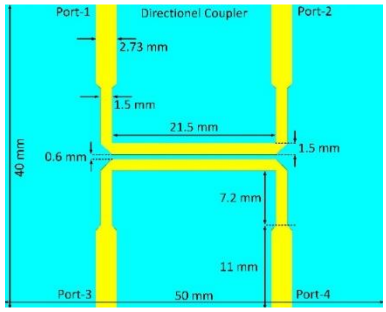

Figure 4. Geometric structure and dimensions of the directional coupler [14].

Based on the equivalent circuit topology of the basic π model of the directional coupler presented in Figure 3, the Equivalent Circuit 1 topology obtained by including additional lumped elements representing the feed lines and structural losses of the physical structure shown in Figure 4 is shown in Figure 6.

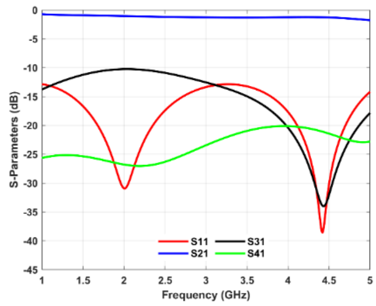

Figure 5. Frequency-dependent variation of S-parameters obtained from the CST simulation [14].

Figure 6 shows L_c, the inductance of the coupling lines of the directional coupler; M, the mutual inductance between the coupling lines; L_f, the inductance of the feed lines; C_{cc}, the capacitive coupling between the coupling lines; C_{cg}, the capacitance between the coupling lines and the ground plane; while C_{fg} represents the capacitance between the feed lines and the ground plane. Additionally, R_{loss} represents losses due to transmission lines and dielectric materials in the structure.

To assess the extent to which this topology aligns with CST simulation data, optimization studies were conducted in the ADS environment for five different scenarios. In this context, ***Scenario 1*** was optimized for the S_{11} parameter, ***Scenario 2*** for the S_{21} parameter, ***Scenario 3*** for the S_{31} parameter, and ***Scenario 4*** for the S_{41} parameter to achieve the best fit. ***Scenario 5*** aims to optimize all S-parameters simultaneously. Table 1 presents a comparative overview of the optimal element values obtained as a result of the optimizations performed for the five different scenarios.

Figure 7-11 details the frequency domain behavior of the *S*-parameters obtained from ADS-based optimization for five different operating scenarios (Scenarios 1-5) defined for the Equivalent Circuit 1 topology of the directional coupler. The optimized *S*-parameters for each operating scenario are presented in comparison with reference CST simulation results to evaluate the model's behavior. This comparison clearly demonstrates the frequency-dependent deviations and changes in the level of fits that arise in the Equivalent Circuit 1 topology under different operating scenarios.

An error analysis was performed to quantitatively evaluate the agreement between the *S*-parameter responses obtained from ADS optimization and the CST simulation data. Table 2 shows the Mean Absolute Error (MAE) calculated for each *S*-parameter for Scenarios 1-5, along with the absolute maximum deviation ($|\Delta S_{mn}|_{max}$) and absolute minimum deviation ($|\Delta S_{mn}|_{min}$) values between the ADS and CST results. Furthermore, the frequency points at which these deviations occur are also indicated in the table. The last row of the table shows the General Average Absolute Error value obtained for the five working scenarios and summarizes the general error trend of the topology.

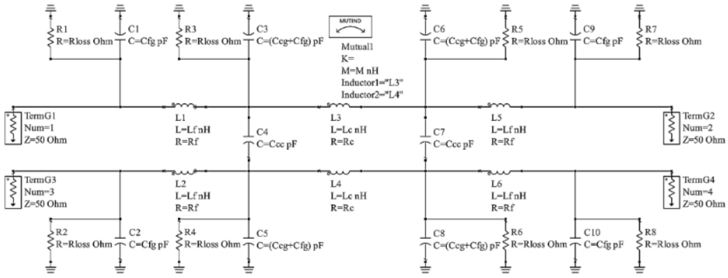

Figure 6. Equivalent Circuit 1 topology of the directional coupler.

Table 1 Values of lumped elements for *S*-parameter optimizations scenarios for Equivalent Circuit 1.

Scenario	C_{cc} (pF)	C_{cg} (pF)	C_{fg} (pF)	L_c (nH)	L_f (nH)	M (nH)	R_c (Ω)	R_f (Ω)	R_{loss} (Ω)	Target Parameter
Scenario 1	0.330	0.160	0.970	3.000	2.280	0.750	0.150	0.900	2400	S_{11}
Scenario 2	0.210	0.060	0.930	2.600	1.850	1.400	1.850	0.050	10000	S_{21}
Scenario 3	1.260	0.340	0.320	1.060	0.650	0.300	0.250	0.300	1200	S_{31}
Scenario 4	0.910	0.400	0.250	0.950	0.380	0.470	1.4×10^{-5}	2.7×10^{-6}	100	S_{41}
Scenario 5	0.340	0.135	0.930	3.000	2.260	0.800	0.150	0.900	3100	$S_{11}, S_{21}, S_{31}, S_{41}$

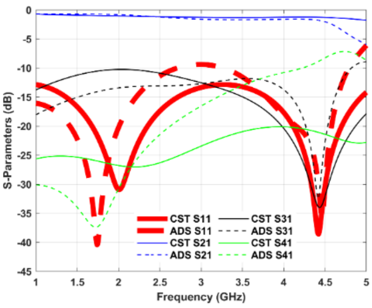

Figure 7. Comparison of the *S*-parameter responses of Equivalent Circuit 1, optimized for S_{11}, with CST data

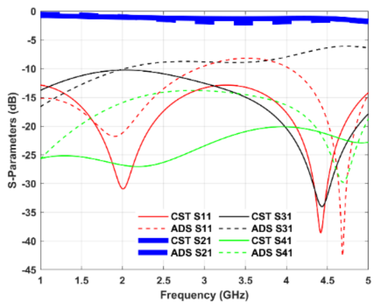

Figure 9. Comparison of the *S*-parameter responses of Equivalent Circuit 1, optimized for S_{31}, with CST data

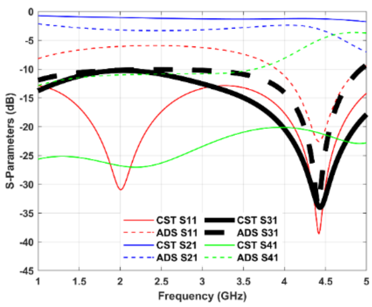

Figure 8. Comparison of the *S*-parameter responses of Equivalent Circuit 1, optimized for S_{21}, with CST data

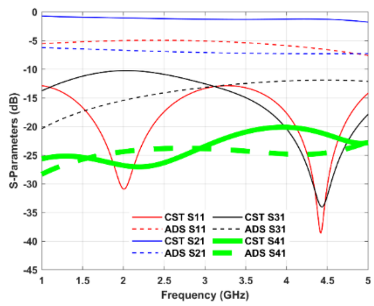

Figure 10. Comparison of the *S*-parameter responses of Equivalent Circuit 1, optimized for S_{41}, with CST data

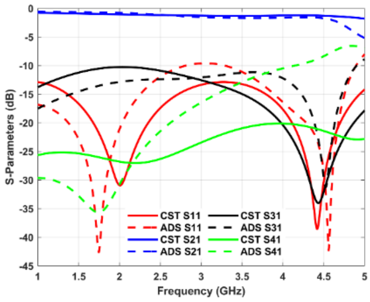

Figure 11. Comparison of the *S*-parameter responses of Equivalent Circuit 1, optimized for all S-parameters, with CST data

The error analysis presented in Table 2 shows that the overall MAE value of the examined topology is 5.64 dB. When we specifically examined the Equivalent Circuit 1 model, it was determined that the overall MAE for Scenario 1 was 4.51 dB. However, the MAE reaching 8.19 dB for the S_{41} parameter reveals that the model performed poorly for this parameter. Although the overall MAE for Scenario 5 is 4.52 dB, which is close to Scenario 1, the error for the S_{41} parameter is 8.10 dB, indicating a high deviation tendency for this parameter. The relatively higher S_{41} deviations observed in this early equivalent circuit topology can be attributed to the inherent balance between the even- and odd-mode phase velocities ($v_{even} \neq v_{odd}$) in the microstrip structure [10], [15]. In a single-segment lumped-element topology, this distributed phase imbalance cannot be adequately captured, as the model assigns a single quasi-static coupling capacitance (C_{cc}) and mutual inductance (M) to represent what is physically a spatially distributed interaction along the coupled line length [16]. Consequently, the destructive interference condition required for high isolation is not reproduced across the full frequency band.

Table 2. Comparison of *S*-Parameters from CST and ADS Simulations for Equivalent Circuit 1: MAE, maximum and minimum error values, and the frequency points at which these errors were observed.

Scenario	Parameter	$\|\Delta S_{mn}\|_{min}$ (dB)	$f_{r,\|\Delta Smn\| min}$ (GHz)	$\|\Delta S_{mn}\|_{max}$ (dB)	$f_{r,\|\Delta Smn\| max}$ (GHz)	MAE (dB)
Scenario 1	**S_{11}**	**0**	**1.878 3.786 4.080 4.458 4.500**	**18.829**	**1.740**	**4.92**
	S_{21}	0	2.242	4.192	4.498	0.53
	S_{31}	0	3.030	11.674	4.468	4.40
	S41	0	2.154	15.478	4.800	8.19
	General MAE for Scenario 1					**4.51**
Scenario 2	S_{11}	0	1.632 4.590	22.447	4.416	5.55
	S_{21}	**0**	**2.124**	**0.712**	**3.486**	**0.36**
	S_{31}	0	1.962	27.481	4.434	7.22
	S_{41}	0	1.008 4.398 4.872	12.367	2.364	6.66
	General MAE for Scenario 2					**4.95**
Scenario 3	S11	4.688	1.002	24.875	2.010	9.70
	S21	**1.131**	**4.020**	**5.256**	**4.998**	**2.01**
	S31	**0**	**1.956**	**9.612**	**4.656**	**3.29**
	S41	**10.508**	**3.594**	**19.253**	**4.902**	**14.17**
	General MAE for Scenario 3					**7.29**
Scenario 4	S11	6.618	4.998	32.098	4.422	13.08
	S21	**5.499**	**4.998**	**6.060**	**4.242**	**5.78**
	S31	0	3.114	22.130	4.434	6.39
	S41	**0**	**1.566 2.934 4.956**	**4.667**	**4.020**	**2.29**
	General MAE for Scenario 4					**6.89**
Scenario 5	**S11**	**0**	**1.884 4.506 4.668**	**20.860**	**1.746**	**5.22**
	S21	0	2.574	3.392	4.998	0.44
	S31	**0**	**2.904 4.518 4.548**	**12.991**	**4.374**	**4.32**
	S41	0	2.160	16.324	4.872	8.10
	General MAE for Scenario 5					**4.52**
General MEA for all scenarios						**5.64**

In addition to the distributed coupling issues, the feed line discontinuities (the physical transition between thick and thin microstrip sections in Figure 4) introduce parasitic reactances that perturb the port impedances[10], [17] . In Equivalent Circuit 1, these discontinuities are represented by a single L_f–C_{fg} section, which is insufficient to capture the frequency-dependent phase shift introduced by the physical step. Therefore, to improve the model, the thick and thin sections of the feed line in the physical structure of the directional coupler (Figure 4) were represented by separate π models and combined with the coupling structure. The equivalent circuit topology obtained from this improved structure is referred to as Equivalent Circuit 2 and is shown in Figure 12.

These results indicate that the Equivalent Circuit 1 model exhibits significant deviations and has limitations in accurately representing the directional coupler. To quantitatively evaluate the compatibility of the Equivalent Circuit 2 topology with the CST-based electromagnetic model, the Scenario 1–5 optimization method, which was defined in detail for Equivalent Circuit 1, was applied in the ADS environment using the same systematic approach. The optimal values of the lumped elements corresponding to each scenario for this topology, shown in Figure 12, were obtained as a result of the optimization process and are presented in Table 3

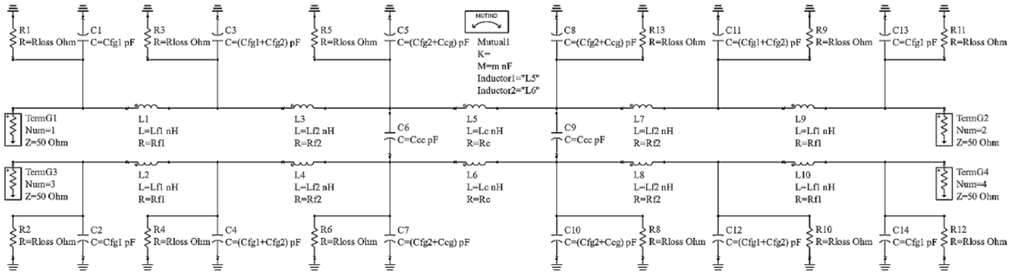

Figure 12. Equivalent Circuit 2 topology of the directional coupler.

Table 3. Lumped element values for S-parameter optimization scenarios for Equivalent Circuit 2.

Scenario	C_{cc} (pF)	C_{cg} (pF)	C_{fg1} (pF)	C_{fg2} (pF)	L_c (nH)	L_{f1} (nH)	L_{f2} (nH)	M (nH)	R_c (Ω)	R_{f1} (Ω)	R_{f2} (Ω)	R_{loss} (Ω)	Target Parameter
Scenario 1	0.183	0.064	0.051	0.655	3.556	1.680	3.647	0.497	$3.5\text{x}10^{-4}$	0.034	0.027	998	S_{11}
Scenario 2	0.347	0.001	0.077	0.635	2.013	1.218	1.576	0.605	$3.5\text{x}10^{-4}$	0.030	0.935	2815	S_{21}
Scenario 3	0.175	0.117	0.047	0.594	2.927	1.581	2.827	0.305	$3.5\text{x}10^{-4}$	0.030	0.658	2428	S_{31}
Scenario 4	0.282	0.360	$2.5\text{x}10^{-5}$	1.111	1.316	$1.5\text{x}10^{-8}$	2.233	0.305	$2.4\text{x}10^{-6}$	$1.7\text{x}10^{-5}$	5.657	334080	S_{41}
Scenario 5	0.175	0.117	0.047	0.594	2.927	1.581	2.827	0.305	$1.1\text{x}10^{-10}$	0.030	0.658	2428	$S_{11}, S_{21}, S_{31}, S_{41}$

Figures 13–17 present the frequency-domain responses of the S-parameters obtained as a result of optimization processes performed on ADS within the scope of five different operating scenarios (Scenarios 1–5) for the Equivalent Circuit 2 topology of the directional coupler. The optimized S-parameters for each scenario are provided in comparison with CST-based reference results to examine the accuracy performance of the model.

These comparisons reveal the frequency-dependent matching behavior exhibited by Equivalent Circuit 2 in different scenarios and the level of improvement achieved compared to the previous topology.

A comprehensive error analysis was applied to quantitatively examine the consistency of S-parameter responses obtained from optimizations performed using Equivalent Circuit 2 in the ADS environment with CST simulation results. In this context, Mean Absolute Error (MAE) values were calculated for each S-parameter for Scenarios 1-5; the maximum absolute deviation ($|\Delta S_{mn}|_{max}$) and minimum absolute deviation ($|\Delta S_{mn}|_{min}$) values between the ADS and CST results were determined.

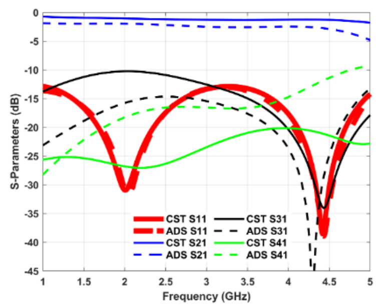

Figure 13. Comparison of the S-parameter responses of Equivalent Circuit 2, optimized for S_{11}, with CST data.

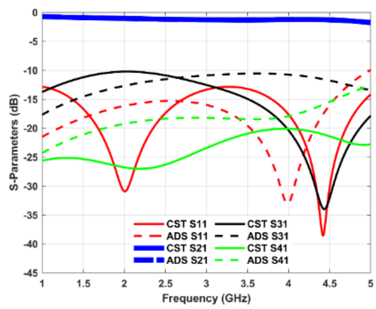

Figure 14. Comparison of the S-parameter responses of Equivalent Circuit 2, optimized for S_{21}, with CST data.

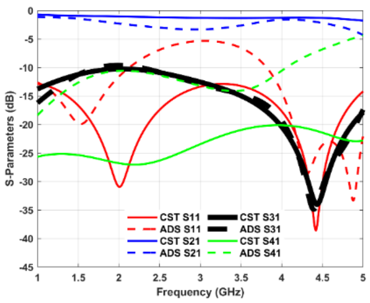

Figure 15. Comparison of the *S*-parameter responses of Equivalent Circuit 2, optimized for S_{31}, with CST data.

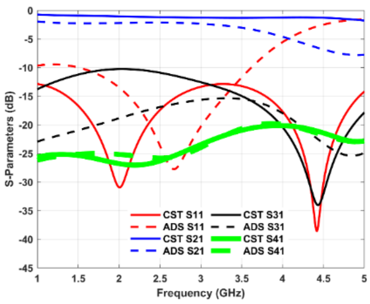

Figure 16. Comparison of the *S*-parameter responses of Equivalent Circuit 2, optimized for S_{41}, with CST data.

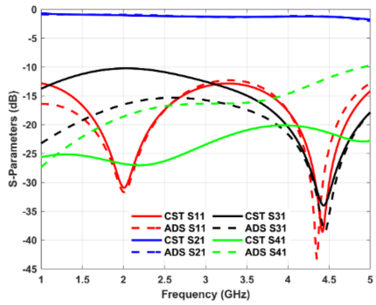

Figure 17. Comparison of the *S*-parameter responses of Equivalent Circuit 2, optimized for all *S*-parameters, with CST data.

Additionally, the frequency points at which these deviations occur have been added to the table, revealing the frequency dependence of the deviations in detail. Table 4 shows the error metrics for all scenarios of Equivalent Circuit 2. The last row of the table shows the General MAE value, which summarizes the general error behavior of the topology.

Table 4. Comparison of *S*-Parameters from CST and ADS Simulations for Equivalent Circuit 2: MAE, maximum and minimum error values, and the frequency points at which these errors were observed

Scenario	Parameter	$\lvert\Delta S_{mn}\rvert_{min}$ (dB)	$f_{r,\lvert\Delta Smn\rvert\,min}$ (GHz)	$\lvert\Delta S_{mn}\rvert_{max}$ (dB)	$f_{r,\lvert\Delta Smn\rvert\,max}$ (GHz)	MAE (dB)
Scenario 1	**S_{11}**	**0**	**1.422 2.004 2.526 3.096 4.380 4.422**	**3.1292**	**4.494**	**0.82**
	S_{21}	0.9091	2.0880	3.1201	5.000	1.27
	S_{31}	0	4.3860	23.2796	4.2960	5.16
	S_{41}	0	1.2300	13.5170	4.9680	6.96
	General MAE for Scenario 1					**3.55**
Scenario 2	S_{11}	0	1.578 2.682 4.218	20.9908	4.4220	6.56
	S_{21}	**0**	**1.068 1.758 3.150 4.254 4.836**	**0.0535**	**3.6780**	**0.02**
	S_{31}	0	2.652	22.4324	4.434	5.65
	S_{41}	1.3043	0.996	10.2536	5.000	5.20
	General MAE for Scenario 2					**4.36**
Scenario 3	S_{11}	0	1.056 1.632 4.176 4.320 4.620	19.5502	2.022	7.14
	S_{21}	0.3264	4.068	2.7153	5.022	1.18
	S_{31}	**0**	**1.506 2.556 3.390 4.188 4.434 4.596 4.974**	**2.4478**	**1.000**	**0.67**
	S_{41}	6.8361	3.564	18.4468	5.000	12.36
	General MAE for Scenario 3					**5.34**

Scenario 4	S_{11}	0	2.370 3.420	35.7617	4.422	10.41
	S_{21}	0.9277	2.592	6.2021	4.836	2.38
	S_{31}	0	3.612 4.674	11.5536	4.422	5.59
	S_{41}	**0**	**1.410** **2.622** **3.318** **4.128**	**1.6782**	**2.094**	**0.5**
	General MAE for Scenario 4					**4.72**
Scenario 5	S_{11}	0	2.568 4.014 4.392	11.7629	4.3500	1.58
	S_{21}	0	1.446 2.808 3.678 4.572	0.2637	5.00	0.07
	S_{31}	0.0217	5.000	9.4726	1.000	4.01
	S_{41}	0	1.1820	13.0739	5.000	6.84
	General MAE for Scenario 5					**3.13**
General MEA for all scenarios						**4.22**

According to the error analysis presented in Table 4, the General Average Absolute Error (MAE) value of 4.22 dB indicates that the Equivalent Circuit 2 topology provides a better fit compared to Equivalent Circuit 1. However, there is still a noticeable deviation between the model and physical reality. Equivalent Circuit 2 is still limited to a high MAE of 6.84 dB for S41, specifically 3.13 dB for Scenario 5.

In the equivalent circuit modeling of transmission lines, dividing the line into short segments is an important approach that increases the accuracy of the model. In the equivalent circuit modeling of the microstrip directional coupler, the Short Line Approach, as defined in transmission line theory, has been adopted. According to the classical microwave transmission line model definition by Pozar, a lossless transmission line segment with physical length l can be represented by lumped elements (L or C) when its electrical length is very short ($\beta l \ll 1$) [10]. Under this condition, the input impedance of the line is approximately accepted as $Z_{in} \approx jZ_0\beta l$, and the line can be modeled as a simple LC circuit. As the operating frequency increases, the line's phase constant β grows and the line's electrical length increases, which limits the accuracy of the single-section LC model. The phase constant is given in Equation (9), taking into account the phase propagation velocity (v_p) of the medium:

$$\beta = \frac{2\pi f}{v_p} \tag{9}$$

When the electrical length exceeds the critical threshold, the single-segment model becomes inadequate to represent the distributed impedance and phase response of the physical line. To overcome this limitation and improve model accuracy, a segmentation approach has been applied in this study.

This method segments transmission lines with a total length of ltotal into N LC cells connected in series. The electrical length of each segment becomes shorter according to the condition given in Equation (10).

$$\theta_{sec} = \beta \frac{l_{total}}{N} << 1 \tag{10}$$

As can be seen from Equation (10), increasing the number of segments by N reduces the electrical length of each segment, thereby decreasing the phase error and improving the accuracy of the equivalent model at high frequencies. Therefore, since the single-segment approach is insufficient for microstrip structures requiring broadband analysis, a segmented structure has been preferred.

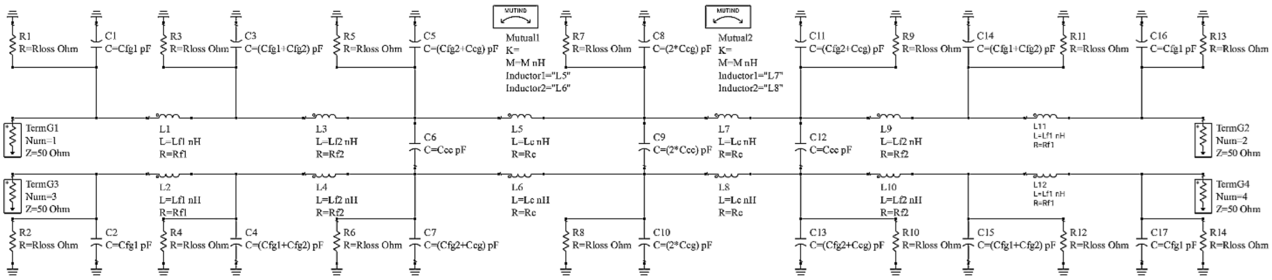

Figure 18. Equivalent Circuit 3 topology of the directional coupler.

Table 5. Lumped element values for *S*-parameter optimization scenarios for Equivalent Circuit 3.

Scenario	C_{cc} (pF)	C_{cg} (pF)	C_{fg1} (pF)	C_{fg2} (pF)	L_c (nH)	L_{f1} (nH)	L_{f2} (nH)	M (nH)	R_c (Ω)	R_{f1} (Ω)	R_{f2} (Ω)	R_{loss} (Ω)	Target Parameter
Scenario 1	0.166	0.270	0.182	0.311	3.146	1.550	2.433	1.283	$1x10^{-5}$	$4x10^{-6}$	$8x10^{-6}$	1460	S_{11}
Scenario 2	0.242	0.361	0.336	0.068	2.010	1.598	2.433	0.600	$9x10^{-6}$	$8x10^{-7}$	$4x10^{-5}$	2485	S_{21}
Scenario 3	0.205	0.386	0.480	0.076	2.732	1.546	0.185	0.814	$1x10^{-7}$	$8x10^{-7}$	$2x10^{-7}$	10390	S_{31}
Scenario 4	0.238	0.534	0.581	0.214	1.984	1.540	0.568	0.530	$5x10^{-6}$	$7x10^{-7}$	$3x10^{-5}$	6968	S_{41}
Scenario 5	0.268	0.503	0.612	0.210	2.146	1.655	0.696	0.657	$1x10^{-5}$	$2x10^{-6}$	$1x10^{-5}$	1680	$S_{11}, S_{21}, S_{31}, S_{41}$

In this study, the coupling lines of the directional coupler are modeled by dividing them into an appropriate number of segments. This segmentation process has extended the validity range of the transmission line approach, more accurately represented behavior over wide frequency ranges, and made the model's optimization process more stable. In this context, the Equivalent Circuit 3 structure obtained by dividing the coupling lines into two parts using the segmentation-based modeling approach is presented in Figure 18.

The previously used five-scenario optimization approach was applied within Equivalent Circuit 3 in the ADS environment, using the same methodological framework. The most suitable values for the lumped elements of this topology within the scope of Scenarios 1–5 were determined through optimization studies, and these values are listed in Table 5.

Figures 19–23 comprehensively illustrate the frequency domain responses of the *S*-parameters obtained through optimization studies conducted in the ADS environment within the scope of Scenarios 1–5 defined for the Equivalent Circuit 3 topology. The optimized *S*-parameters for each study scenario are presented in comparison with CST reference outputs to reveal the extent to which the model represents the electromagnetic behavior. This evaluation clearly shows the changes in the frequency-dependent performance of Equivalent Circuit 3 and the differences in compliance between the scenarios.

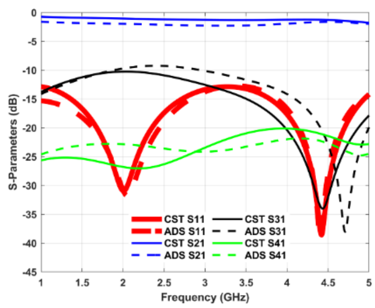

Figure 19. Comparison of the *S*-parameter responses of Equivalent Circuit 3, optimized for S_{11}, with CST data.

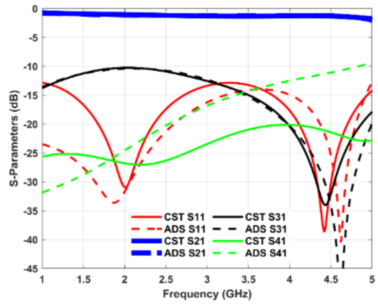

Figure 20. Comparison of the *S*-parameter responses of Equivalent Circuit 3, optimized for S_{21}, with CST data.

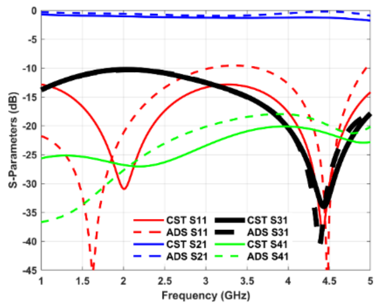

Figure 21. Comparison of the *S*-parameter responses of Equivalent Circuit 3, optimized for S_{31}, with CST data.

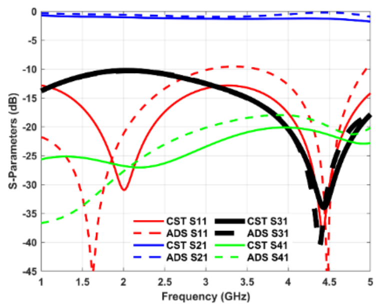

Figure 22. Comparison of the *S*-parameter responses of Equivalent Circuit 3 optimized for S_{41} with CST data

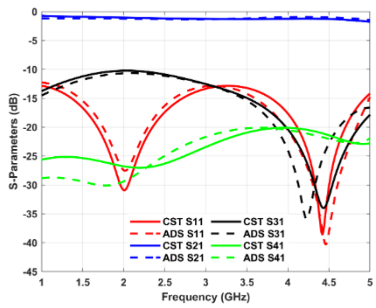

Figure 23. Comparison of the *S*-parameter responses of Equivalent Circuit 3, optimized for all *S*-parameters, with CST data

Table 6 Comparison of *S*-Parameters from CST and ADS Simulations for Equivalent Circuit 3: MAE, maximum and minimum error values, and the frequency points at which these errors were observed.

Scenario	Parameter	$\lvert\Delta S_{mn}\rvert_{min}$ (dB)	$f_{r,\lvert\Delta Smn\rvert min}$ (GHz)	$\lvert\Delta S_{mn}\rvert_{max}$ (dB)	$f_{r,\lvert\Delta Smn\rvert max}$ (GHz)	MAE (dB)
Scenario 1	**S_{11}**	**0**	**1.836 2.004 3.228 4.338 4.422 4.974**	**2.992**	**2.142**	**1.13**
	S_{21}	0.1854	5.000	0.9845	3.030	0.78
	S_{31}	0	1.692 4.596	14.3839	4.710	0.19
	S_{41}	0	2.8920	4.0391	2.106	2.07
	General MAE for Scenario 1					**1.04**
Scenario 2	S_{11}	0	3.660 4.536 4.908	17.4896	4.620	5.17
	S_{21}	**0**	**2.532 4.848**	**0.3004**	**5.000**	**0.06**
	S_{31}	0	1.458 2.322 3.258 3.990 4.482	26.4369	4.620	1.53
	S_{41}	0	1.818	13.3426	4.998	6.57
	General MAE for Scenario 2					**3.33**
Scenario 2	S_{11}	0	1.860 4.452 4.554	26.2882	1.626	6.35
	S_{21}	0.3436	3.018	1.0871	4.620	0.57
	S_{31}	**0**	**2.274 3.120 3.666 4.044 4.446 4.986**	**7.9705**	**4.374**	**0.54**
	S_{41}	0	2.076	11.0601	1.020	3.6
	General MAE for Scenario 3					**2.77**
Scenario 4	S_{11}	0	2.094 2.538 4.542	38.1670	4.656	4.51
	S_{21}	0.0320	1	1.3324	5.000	0.62
	S_{31}	0	4.446 4.956	6.6958	4.362	1.26
	S_{41}	**0**	**1.278 1.968 2.700 3.528 4.458 4.818**	**0.3607**	**2.328**	**0.01**
	General MAE for Scenario 4					**1.6**
Scenario 5	S_{11}	0	3.180 4.380 4.428	7.9016	4.506	1.86
	S_{21}	0.0013	3.204	0.4369	1	0.22
	S_{31}	0	4.3320	10.0638	4.2180	1.81
	S_{41}	0	1.848 2.634 4.446	44.0309	1	3.74
	General MAE for Scenario 5					**1.91**
General MEA for all scenarios						**2.29**

For Equivalent Circuit 3, the same error analysis study was performed as for the previous equivalent circuits; the results are presented in Table 6

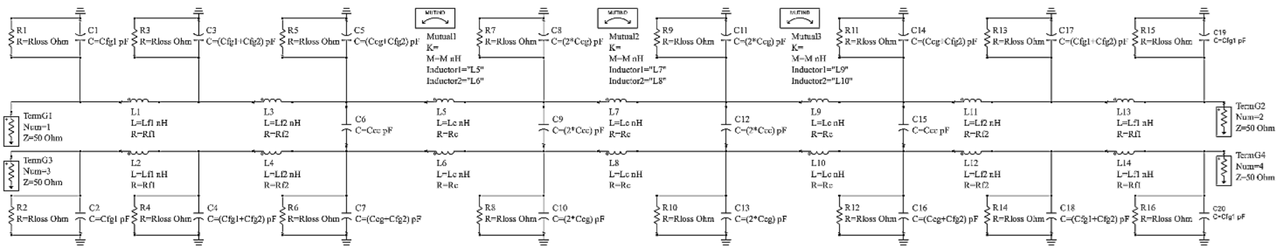

Figure 24. Equivalent Circuit 4 topology of the directional coupler.

Table 7. Lumped element values for *S*-parameter optimization scenarios for Equivalent Circuit 4.

Scenario	C_{cc} (pF)	C_{cg} (pF)	C_{fg1} (pF)	C_{fg2} (pF)	L_c (nH)	L_{f1} (nH)	L_{f2} (nH)	M (nH)	R_c (Ω)	R_{f1} (Ω)	R_{f2} (Ω)	R_{loss} (Ω)	Target Parameter
Scenario 1	0.178	0.314	0.666	0.102	1.369	1.638	0.409	0.434	2.2×10^{-6}	6.444	1.246	53506	S_{11}
Scenario 2	0.098	0.245	0.113	0.224	2.651	0.864	0.601	0.324	0.043	1.186	0.250	5712	S_{21}
Scenario 3	0.176	0.331	0.647	0.204	1.457	1.630	0.664	0.438	2.4×10^{-5}	0.009	1.244	2477	S_{31}
Scenario 4	0.175	0.312	0.372	0.322	1.514	1.025	1.020	0.473	0.044	2.472	0.378	6006	S_{41}
Scenario 5	0.189	0.314	0.359	0.315	1.568	1.011	0.994	0.513	0.046	2.548	0.473	3696	$S_{11}, S_{21}, S_{31}, S_{41}$

According to the error analysis summarized in Table 6, the overall MAE value of 2.29 dB indicates that the Equivalent Circuit 3 topology provides a better fit compared to Equivalent Circuit 2. However, there is still a slightly limited deviation between the model and physical reality. Equivalent Circuit 3 yielded the most successful optimization result with a low MAE of 1.04 dB in Scenario 1. The highest MAE observed in Scenario 1 was 2.07 dB for the S_{41} parameter

It has been observed that Equivalent Circuit 3, created by dividing the coupling line into two sections, yields more successful results compared to previous topologies. This finding demonstrates that modeling the electromagnetic interactions occurring along the line on a regional basis significantly increases the accuracy level. Therefore, it has been confirmed that the proposed approach of dividing the coupling line into smaller segments improves the model's fit and produces more consistent results. Following this improvement, a further step was taken by dividing the coupling line into three sections, resulting in the Equivalent Circuit 4 topology presented in Figure 24.

As with previous equivalent circuit topologies, the optimal values of the lumped elements for the Equivalent Circuit 4 model, shown in Figure 24, were determined through ADS optimization studies conducted separately for Scenarios 1–5. These lumped element values corresponding to each scenario are presented comparatively in Table 7.

Figures 25–29 detail the frequency domain characteristics of the *S*-parameters obtained from ADS-based optimizations for Scenarios 1–5, as they relate to the Equivalent Circuit 4 topology of the directional coupler. The optimized *S*-parameters for each scenario are presented in comparison with CST simulation results during the model validation process. This comprehensive comparison enables the evaluation of the frequency-dependent performance of Equivalent Circuit 4 under different operating conditions. Clearly, it demonstrates the changes in the topology's representational capability compared to previous models.

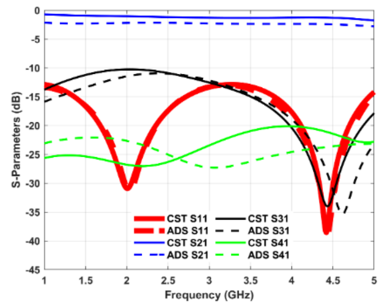

Figure 25. Comparison of the *S*-parameter responses of Equivalent Circuit 4, optimized for S_{11}, with CST data.

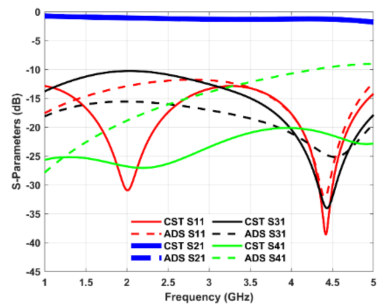

Figure 26. Comparison of the *S*-parameter responses of Equivalent Circuit 4, optimized for S_{21}, with CST data.

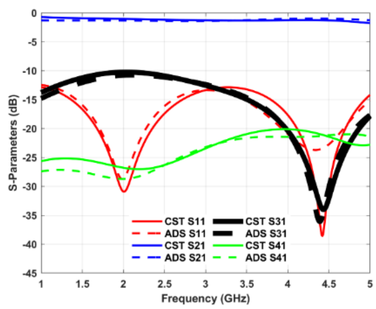

Figure 27. Comparison of the *S*-parameter responses of Equivalent Circuit 4, optimized for S_{31}, with CST data.

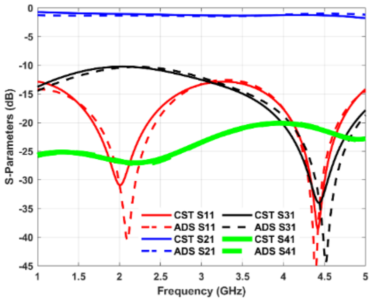

Figure 28. Comparison of the *S*-parameter responses of Equivalent Circuit 4, optimized for S_{41}, with CST data.

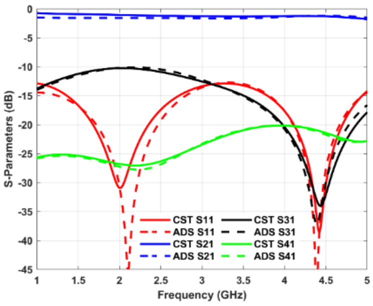

Figure 29. Comparison of the *S*-parameter responses of Equivalent Circuit 4, optimized for all *S*-parameters, with CST data.

The error analysis procedure applied to previous equivalent circuit topologies has been reapplied to Equivalent Circuit 4 with the same scope and criteria to ensure methodological consistency. In this context, the MAE and frequency-based deviation values ($|\Delta S_{mn}|_{max}$ and $|\Delta S_{mn}|_{min}$) between the *S*-parameter responses obtained as a result of ADS optimization and the CST reference data were calculated in detail for all scenarios. All quantitative results obtained are presented comparatively in Table 8.

According to the error analysis summarized in Table 8, the General MAE value of 1.64 dB indicates that the Equivalent Circuit 4 topology approximates the physical model with higher accuracy than the previous equivalent circuits. This result demonstrates that modeling the coupling line by dividing it into three parts allows for a more accurate representation of the electromagnetic interactions occurring along the line

.

Table *8*. Comparison of S-Parameters from CST and ADS Simulations for Equivalent Circuit 4: MAE, maximum and minimum error values, and the frequency points at which these errors were observed.

Scenario	Parametre	$\|\Delta S_{mn}\|_{min}$ (dB)	$f_{r,\|\Delta Smn\| min}$ (GHz)	$\|\Delta S_{mn}\|_{max}$ (dB)	$f_{r,\|\Delta Smn\| max}$ (GHz)	MAE (dB)
Scenario 1	**S_{11}**	**0**	**1.434 2.004 2.520 3.114 4.362 4.428**	**3.1253**	**4.482**	**0.72**
	S_{21}	0.9828	2.736	1.4309	1.098	1.13
	S_{31}	0	2.556 4.512	9.2365	4.650	2.03
	S_{41}	0	2.622	5.2851	3.480	3.20
	General MAE for Scenario 1					**1.77**
Scenario 2	S_{11}	0	1.386 3.576 4.140	18.0786	2.010	3.67
	S_{21}	**0**	**1.020 1.878 3.246 4.884**	**0.0342**	**1.308**	**0.01**
	S_{31}	0	4.062 4.704	9.2169	4.428	4.01
	S_{41}	0	1.236	13.8723	4.926	8.51
	General MAE for Scenario 2					**4.05**
Scenario 3	**S_{11}**	0	3.000 4.218 4.740	15.1194	4.4220	1.86
	S_{21}	0	3.3480	0.5624	1.000	0.27
	S_{31}	**0**	**2.796 3.930 4.446**	**3.5052**	**4.3620**	**0.54**
	S_{41}	0	2.508 3.156 4.458	2.2527	1.7340	1.11
	General MAE for Scenario 3					**0.95**

Scenario 4	S_{11}	0	1.470 2.004 2.958 4.044 4.422 4.908	14.0700	4.3920	1.34
	S_{21}	0	3.864	0.5942	5.000	0.26
	S_{31}	0	2.160 4.446	13.2949	4.518	1.16
	S_{41}	**0**	**1.386 2.064 3.900 4.626**	**0.3389**	**2.436**	**0.09**
	General MAE for Scenario 4					**0.71**
Scenario 5	S_{11}	0	1.536 2.004 3.144 4.014 4.422 4.926	25.9168	4.386	1.58
	S_{21}	0	4.260	0.4369	1.000	0.22
	S_{31}	0	1.926 3.270 4.452	4.4805	4.3740	0.64
	S_{41}	0	2.826 3.894 4.902	0.7273	2.2860	0.23
	General MAE for Scenario 5					**0.67**
General MEA for all scenarios						**1.64**

The success of this segmentation strategy is most notably reflected in the isolation parameter. Under simultaneous multi-parameter optimization (Scenario 5), the S41 MAE dramatically decreases from 8.10 dB in Equivalent Circuit 1 to an impressive 0.23 dB in the final Equivalent Circuit 4 topology, representing a 97.1% reduction in isolation error. Equivalent Circuit 4 yielded the most successful optimization result for Scenario 5 with a low overall MAE value of 0.67 dB. However, the 1.58 dB error observed for the S_{11} parameter in Scenario 5 indicates that the model may contain minor deviations in the specific frequency ranges.

Results and Discussion

In this study, the performance of equivalent circuit topologies developed to model the electromagnetic behavior of a microstrip directional coupler was evaluated using CST Studio Suite reference data, optimization Scenarios 1–5 performed in the ADS environment, and calculated Mean Absolute Error metrics. Starting from the basic π model (Equivalent Circuit 1), a systematic decrease in modelling error was observed up to the final model (Equivalent Circuit 4), which was developed by segmenting the transmission line and modelling structural effects.

Upon examining the quantitative data, the overall MAE of the single-section basic structure (Equivalent Circuit 1) at 4.52 dB decreased to 1.04 dB in the Equivalent Circuit 3 structure, where the coupling lines of the directional coupler were divided into multiple sections; while in the final Equivalent Circuit 4 structure, it was observed to have dropped to an extremely low level of 0.67 dB. In particular, the 0.64 dB error rate obtained for S_{21} in the final model and the success in tracking resonance in the S_{11} parameter demonstrate that the model successfully represents the physical structure over a wide bandwidth.

In the field of microwave engineering, an amplitude error margin of less than ±1 dB is generally recognized as a stringent and highly acceptable accuracy threshold for lumped-element equivalent circuit models. Notably, recent studies in the literature, such as the one focusing on GaN-based power dividers [9], report a deviation of approximately 0.7 dB between simulation and measurement as a successful agreement. The reduction of our model's overall MAE from 4.52 dB to a highly suppressed level of 0.67 dB indicates that the proposed final topology not only aligns with these strict practical standards but actually exceeds them, confirming the high fidelity of the segmentation-based modeling approach.

In addition to these successful results, the comparison of optimization scenarios raises important points of discussion regarding the physical consistency of the model. In analyses conducted on the basic topologies (Equivalent Circuits 1 and 2), it was observed that Scenario 2, which targeted only the S_{21} parameter, reduced the S_{21} error to a low level of 0.36 dB, but increased the S_{41} error to a high level of 6.66 dB. In contrast, Scenario 1, which targets only S_{11}, achieved a surprisingly high overlap in Scenario 5, where all parameters were optimized. This situation demonstrates that focusing on a single parameter in the equivalent circuit modelling of a directional coupler can lead to a disconnect from physical reality, but that impedance matching (S_{11}) is a dominant and decisive factor for structural consistency.

In single-objective optimization scenarios, the algorithm strictly focuses on minimizing the error function of the selected S-parameter while disregarding the others. This leads to lumped element values being driven to physically unrealistic extremes in an attempt to compensate for the distributed electromagnetic effects that are inadequately captured by the model.

For instance, under Scenario 4 in Equivalent Circuit 2, where only the isolation parameter (S_{41}) is optimized, the fringing capacitance is forced down to C_{fg} = 2.483 x 10^{-5} pF, while the conductor loss resistances are reduced to near-zero, physically non-realistic values such as R_{f1} = 1.77 x 10^{-5} Ω and R_c = 2.38 x 10^{-6} Ω.

Although such mathematically forced values improve the targeted *S*-parameter, they compromise the overall physical consistency of the model, resulting in increased errors in the remaining *S*-parameters. In contrast, multi-objective optimization (e.g., Scenario 5), which simultaneously considers all *S*-parameters, yields solutions within a more physically meaningful and balanced parameter space, thereby significantly improving the overall model accuracy.

To clearly demonstrate the fundamental contribution of the proposed multi-section modeling approach, a progressive comparison of all equivalent circuit generations under Scenario 5 is provided in Table 9.

Table 9. Progressive reduction in Mean Absolute Error (MAE) and total percentage improvement across all equivalent circuit topologies under Scenario 5.

Equivalent Circuit	**S_{11} MAE (dB)**	**S_{21} MAE (dB)**	**S_{31} MAE (dB)**	**S_{41} MAE (dB)**	**Overall MAE**
Equivalent Circuit 1	5.22	0.44	4.32	8.10	4.52
Equivalent Circuit 2	1.58	0.07	4.01	6.84	3.13
Equivalent Circuit 3	1.86	0.22	1.81	3.74	1.91
Equivalent Circuit 4	1.58	0.22	0.64	0.23	0.67
Total Improvement (%)	**69.73%**	**50.00%**	**85.19%**	**97.16%**	**85.18%**

As numerically summarized in the last row of Table 9, the transition from a single-section model to the final four-section topology yielded a significant overall error reduction of 85.18%. This global improvement is clearly observed across the entire scattering matrix, with remarkable error reductions of 69.73% in reflection (S_{11}), 50.00% in forward transmission (S_{21}), 85.19% in coupling (S_{31}), and 97.16% in isolation (S_{41}). These progressive results confirm that the proposed segmentation strategy successfully captures the complex and distributed electromagnetic interactions that are typically lost in conventional single-section lumped-element models.

To further clarify the validity range and robustness of the proposed final model (Equivalent Circuit 4), a frequency-subband-based error evaluation was conducted. The operational bandwidth (1.0–5.0 GHz) was divided into three regions: Low-Frequency (1.0–2.3 GHz), Mid-Frequency (2.3–3.6 GHz), and High-Frequency (3.6–5.0 GHz). The recalculated MAE values for each scattering parameter under Scenario 5 are summarized in Table 10.

As shown in Table 10, the proposed topology maintains high fidelity across all sub-regions. The model demonstrates exceptional accuracy in the mid-frequency band, achieving an overall MAE of 0.39 dB. In the high-frequency region (3.6–5.0 GHz), where phase variations and distributed electromagnetic effects are more pronounced, the overall MAE remains at a robust level of 0.73 dB.

Table 10. Subband MAE evaluation for the final model (Equivalent Circuit 4, Scenario 5).

Parameter	**Low-Frequency MAE (1.0-2.3 GHz)**	**Mid-Frequency MAE (2.3-3.6 GHz)**	**High-Frequency MAE (3.6-5.0 GHz)**	**Full Band MAE (1.0-5.0 GHz)**
S_{11} MAE (dB)	2.64	0.80	1.30	**1.58**
S_{21} MAE (dB)	0.35	0.22	0.09	**0.22**
S_{11} MAE (dB)	0.20	0.30	1.42	**0.64**
S_{41} MAE (dB)	0.33	0.23	0.13	**0.23**
Overall MAE	**0.88**	**0.39**	**0.73**	**0.67**

This stable error behavior in the upper frequency band confirms the broadband validity and consistent physical representation capability of the final equivalent circuit model

Conclusion

In this study, a high-accuracy, wide-band equivalent circuit model has been developed for the directional coupler structure, which is of critical importance in microwave sensor applications. During the modelling process, a four-stage systematic optimization approach based on the 'line-splitting principle' was applied to represent the physical behavior of the structure.

Analyses revealed that simple L-C topologies were insufficient. Equivalent Circuit 4, created by extending the equivalent circuit model with lumped elements representing EM interactions using the transmission line segmentation method, showed excellent agreement with electromagnetic simulation results. Indeed, the modelling error, which was approximately 4.5 dB in the initial models, was reduced to 0.67 dB with the proposed model.

These results demonstrate that the proposed approach successfully combines the high accuracy provided by full-wave electromagnetic simulations with the speed of circuit simulators. Consequently, this work offers an effective solution that reduces time costs, particularly in the design and optimization processes of complex microwave systems.

Ethics committee approval and conflict of interest statement

There is no need to obtain permission from the ethics committee for the article prepared.

The authors have declared that the Scientific Research Projects Coordination Unit of Süleyman Demirel University provided the equipment and materials. Furthermore, the authors declare that there are no conflicts of interest or personal relationships that could influence the work reported in this article.

Authors' Contributions

Genç: Writing – review & editing, Writing – original draft, Software, Resources, Methodology, Conceptualization.

Gözel: Writing – review & editing, Writing – original draft, Software, Resources, Methodology, Conceptualization.

Kahriman: Writing – review & editing, Visualization, Formal analysis, Methodology, Conceptualization, Supervision.

Acknowledgement

This study was supported by the Scientific Research Projects Coordination Unit of Süleyman Demirel University under project code FDK-2024-9533. The authors would like to thank the Scientific Research Projects Coordination Unit of Süleyman Demirel University for their support

References

[1] W. Il Chang, M. J. Chung, and C. S. Park, "Compact high-directivity contra-directional coupler," *Electronics (Switzerland)*, vol. 11, no. 24, Dec. 2022, doi: 10.3390/electronics11244115.

[2] A. Eroglu and D. Rönnow, "Design of multilayer and multiline microstrip directional coupler with closed form relations," *Prog. Electromagn. Res. C*, vol. 83, pp. 243–257, 2018.

[3] A. Pourzadi, A. R. Attari, and M. S. Majedi, "A directivity-enhanced directional coupler using epsilon negative transmission line," *IEEE Trans. Microw. Theory Tech.*, vol. 60, no. 11, pp. 3395–3402, 2012, doi: 10.1109/TMTT.2012.2216283.

[4] S. Lee and Y. Lee, "A design method for microstrip directional couplers loaded with shunt inductors for directivity enhancement," *IEEE Trans. Microw. Theory Tech.*, vol. 58, no. 4, pp. 994–1002, Apr. 2010, doi: 10.1109/TMTT.2010.2042544.

[5] T. Hu *et al.*, "Design and simulation of microstrip directional coupler with tight structure and high directivity," in *Proceeding of PAC*, Vancouver, BC, Canada, 2009,pp. 1677–1679.

[6] S. H. Abdelnaby, "Lumped element transdirectional and codirectional coupler," M.S. thesis, Queen's Univ., Kingston, ON, Canada, 2018.

[7] Y. Zhou and Y. Chen, "Lumped-Element Equivalent Circuit Models for Distributed Microwave Directional Couplers," in *International Conference on Microwave and Millimeter Wave Technology*, IEEE, 2008. doi: 10.1109/ICMMT.2008.4540421.

[8] Ö. Kasar, "Theoretical design and implementation of equal and unequal split ultra-wide band Wilkinson power divider with Chebyshev impedance transform," *Journal of Electrical Engineering*, vol. 75, no. 5, pp. 383–391, Sep. 2024, doi: 10.2478/jee-2024-0046.

[9] B. Dökmetaş and M. Karahan, "X-bant haberleşme sistemlerine yönelik küçültülmüş GaN temelli eşit bölen wilkinson güç bölücü," *Osmaniye Korkut Ata Üniversitesi Fen Bilimleri Enstitüsü Dergisi*, vol. 8, no. 1, pp. 432–444, Jan. 2025, doi: 10.47495/okufbed.1499141.

[10] D. M. Pozar, *Microwave Engineering*, Fourth Edition. United States of America: John Wiley & Sons, Inc., 2012.

[11] Ramesh. Garg and I. J. . Bahl, *Microstrip lines and slotlines*. Artech House, Inc, 2024.

[12] A. Eroglu and J. K. Lee, "The complete design of microstrip directional couplers using the synthesis technique," *IEEE Trans. Instrum. Meas.*, vol. 57, no. 12, pp. 2756–2761, 2008, doi: 10.1109/TIM.2008.926391.

[13] I. J. . Bahl, *Lumped elements for RF and microwave circuits*. Artech House, 2003.

[14] İ. Genç, M. A. Gözel, and M. Kahriman, "Microwave sensor design with directional coupler-based CSRR structure for the characterization of the dielectric properties of solid materials," *Measurement*, vol. 259, p. 119548, Feb. 2026, doi: 10.1016/j.measurement.2025.119548.

[15] R. E. . Collin, *Foundations for microwave engineering*, 2nd ed. IEEE Press, 2015.

[16] J.-S. Hong, *Microstrip Filters for RF/Microwave Applications*, 2nd ed. Hoboken, New Jersey.: John Wiley & Sons, Inc, 2011.

[17] K. C. . Gupta, *Microstrip lines and slotlines*. Artech House, 1996.